

High Symmetry of Visual Acuity and Visual Fields in *RPGR*-Linked Retinitis Pigmentosa

Julia-Sophia Bellingrath,¹⁻³ G. Alex Ochakovski,^{1,2} Immanuel P. Seitz,^{1,2} Susanne Kohl,² Eberhart Zrenner,^{1,2} Nicola Hanig,⁴ Holger Prokisch,⁵ Bernhard H. Weber,⁶ Susan M. Downes,^{3,7} Simon Ramsden,⁸ Robert E. MacLaren,^{3,7,9} and M. Dominik Fischer¹⁻³

¹University Eye Hospital, Centre for Ophthalmology, University Hospital Tübingen, Tübingen, Germany

²Institute for Ophthalmic Research, Centre for Ophthalmology, University Hospital Tübingen, Tübingen, Germany

³Nuffield Laboratory of Ophthalmology, Nuffield Department of Clinical Neurosciences, University of Oxford, Oxford, United Kingdom

⁴Centre for Genomics and Transcriptomics, Tübingen, Germany

⁵Institute of Human Genetics, Helmholtz Zentrum München, Munich, Germany

⁶Institute of Human Genetics, University of Regensburg, Regensburg, Germany

⁷Oxford Eye Hospital, Oxford University Hospitals, NHS Foundation Trust, United Kingdom

⁸Manchester Centre for Genomic Medicine, Central Manchester University Hospitals, NHS Foundation Trust, United Kingdom

⁹Moorfields Eye Hospital NHS Foundation Trust, United Kingdom

Correspondence: M. Dominik Fischer, University Eye Hospital, Centre for Ophthalmology, Elfriede-Aulhorn-Str. 5-7, 72076 Tübingen, Germany; Dominik.Fischer@uni-tuebingen.de.

Submitted: April 20, 2017

Accepted: July 20, 2017

Citation: Bellingrath J-S, Ochakovski GA, Seitz IP, et al. High symmetry of visual acuity and visual fields in *RPGR*-linked retinitis pigmentosa. *Invest Ophthalmol Vis Sci*. 2017;58:4457-4466. DOI:10.1167/iovs.17-22077

PURPOSE. Mutations in retinitis pigmentosa GTPase regulator (*RPGR*) cause 70% to 90% of X-linked retinitis pigmentosa (XLRP3) cases, making this gene a high-yield target for gene therapy. This study analyzed the utility of relevant clinical biomarkers to assess symmetry and rate of progression in XLRP3.

METHODS. A retrospective, cross-sectional analysis of 50 XLRP3 patients extracted clinical data including visual acuity (VA), visual fields (I4e and III4e targets), foveal thickness, and ERG data points alongside molecular genetic data. Symmetry was assessed by using linear regression analysis. Kaplan-Meier survival curves (KMCs) and generalized linear mixed model calculations were used to describe disease progression.

RESULTS. Ninety-six percent of patients exhibited a rod-cone phenotype, and 4% a cone-rod phenotype. Open reading frame 15 (ORF15) was confirmed as a mutational hotspot within *RPGR* harboring 73% of exonic mutations. Significant variability, but no clear genotype-phenotype relationship, could be shown between mutations located in exons 1-14 versus ORF15. All biomarkers suggested a high degree of symmetry between eyes but demonstrated different estimates of disease progression. VA and foveal thickness, followed by perimetry III4e, were the most useful endpoints to evaluate progression. KMC estimates predicted a loss of 6/6 vision at a mean of 34 years (± 2.9 ; 95% confidence interval).

CONCLUSIONS. XLRP3 affects retinal structure and function symmetrically, supporting the use of the fellow eye as an internal control in interventional trials. VA and kinetic visual fields (III4e) seem promising functional outcome measures to assess disease progression. KMC analysis predicted the most severe decline in vision between the third and fourth decade of life.

Keywords: retinitis pigmentosa, retinitis pigmentosa GTPase regulator (*RPGR*), gene therapy, disease progression

Retinitis pigmentosa (RP) comprises a group of monogenic disorders that occur with a frequency of 1:4000.^{1,2} The X-linked form of RP (XLRP) is a severe type of RP^{3,4} and when compared to patients with the autosomal dominant form of RP, loss of vision in XLRP patients occurs 30 years earlier.⁴ From 70% to 90% of XLRP cases, and therefore 10% to 20% of RP cases, result from mutations in the retinitis pigmentosa GTPase regulator (*RPGR*) gene,^{5,6} a gene that maps to the RP3 locus on chromosome Xp11.4.^{7,8} XLRP due to mutations in *RPGR* is therefore also termed "X-linked retinitis pigmentosa" (XLRP3). *RPGR* gives rise to several transcript isoforms. Aside from the constitutive variant *RPGR*^{Exon1-19}, which is widely expressed throughout the body,⁷⁻⁹ over 10 splice variants of *RPGR* exist.¹⁰⁻¹³ The *RPGR*^{ORF15} variant is abundantly expressed in

the retina^{8,14-17} where it is localized at the connecting cilium of the photoreceptors^{11,18} and interacts with several proteins through a regulator of chromosome condensation (RCC1)-like domain at its N-terminus, most notably the *RPGR*-interacting protein (RPGRIP1).¹⁹ *RPGR*^{ORF15} shares exons 1-14 and part of exon 15 with *RPGR*^{Exon1-19}, which includes the abovementioned RCC1-like domain at the N-terminus, but *ORF15*, the terminal exon, is unique to *RPGR*^{ORF15}. *ORF15* is a purine-rich, repetitive sequence that codes for a glycine- and glutamic acid-rich protein sequence. Previous publications show that up to 60% of mutations cluster on this terminal exon, which takes up slightly less than half the exonic nucleotide sequence.^{8,20}

RPGR mutations exhibit a notoriously diverse phenotype, which results in a wide range of disease courses. Typically, it



presents as a rod-cone degeneration pattern, although a minority of patients can present with a cone-rod phenotype.²¹ Multiple previous reports¹ find that patients with *ORF15* mutations present with a cone-rod pattern of degeneration. This diversity can partly be explained through allelic heterogeneity, but the variability persists in patients with the same mutation²² and has even been described in (dizygotic) twins.²³ Genetic modifiers have been proposed to account for this, and two specific single nucleotide polymorphism (SNP) changes may be associated with severe disease.²²

Owing to the high prevalence of *RPGR*^{ORF15} mutations in XLRP, the gene represents a high-yield therapeutic target. Several promising preclinical trials to replace *RPGR*^{ORF15} in animal models have already been published.^{1,24–26} To achieve optimal application when potential treatments are brought to clinical trials, it is necessary to thoroughly analyze patient cohorts to determine their pretreatment characteristics. This study aimed to answer three questions: (1) Is XLRP symmetrical between eyes and can the contralateral eye therefore be used as an internal control in an interventional trial? (2) Which parameter is the most sensitive and robust outcome measure to reliably detect treatment safety and/or efficacy? (3) And lastly, is it possible to characterize the dynamic of disease progression to determine the optimal therapeutic window?

MATERIALS AND METHODS

Patient Characteristics

In this retrospective, cross-sectional study, 100 eyes of 50 patients with XLRP resulting from mutations in the *RPGR* gene were analyzed. Patients were referred to and seen at the University Eye Hospital Tübingen and the Oxford Eye Hospital between 2006–2015 and include all genetically confirmed *RPGR* patients evaluated during this interval at both locations. A systematic review of both institutions databases was performed and data points pertaining to visual acuity (VA), visual fields, electroretinography (ERG), and foveal thickness were extracted. Patients were subdivided into rod-cone phenotype, cone-rod phenotype, or rod-cone phenotype with split fovea where the centripetal degeneration encroaches on the fovea. The study was performed in accordance with the tenets of the Declaration of Helsinki 1975 (1983 revision). Institutional review board approval was obtained for genetic testing.

Molecular Assessment

All genetically tested participants gave written consent, approved by the local research and ethical review boards. Genomic DNA was extracted from peripheral blood samples by using standard protocols. Genetic testing was performed at the Centre for Genetics and Transcriptomics (CeGaT GmbH), as well as the molecular genetics laboratories in Tübingen, Regensburg, and München. Research and diagnostic genetic setups in the aforementioned laboratories included single-strand conformation polymorphism analysis, high-resolution melting curve analysis, Sanger sequencing, and next-generation sequencing. Sanger sequencing of PCR-amplified genomic DNA confirmed mutations.^{5,20} Analysis extent and depth was variable, ranging from Sanger sequencing of only *ORF15* of the *RPGR* gene, analysis of all coding exons of *RP2* and *RPGR* (including *ORF15*), as well as panel sequencing of all inherited retinal dystrophy genes.^{5,20,27} Mutations were categorized as missense, nonsense, insertions, deletions, gross deletions, and splice defects. Exonic mutations were further characterized by mutation location, with *ORF15* mutations considered distinct from mutations occurring in exons 1–14.

Clinical Examinations

Visual Acuity. Measurement of VA was performed by using Snellen charts. If VA improved with pinhole, the pinhole-corrected data point was used. Decimal Snellen VA was converted to logMAR by using the formula $\log\text{MAR} = -\log(\text{decimal acuity})$.²⁸

Visual Fields. Visual fields were tested with semiautomated kinetic perimetry with an Octopus 900 or Goldmann perimeter (Haag-Streit, Koeniz, Switzerland) as described previously.^{29,30} The peripheral visual field boundary and blind spot were assessed by using I4e and III4e targets. For the patient cohort from Tübingen, the visual field area (degree²) for I4e and III4e targets was calculated by using the proprietary software's built-in measurement tool. The visual fields of Oxford patients were scanned and assessed with ImageJ (version 2.0.0-rc-30/1.49s, <http://imagej.nih.gov/ij/>; provided in the public domain by the National Institutes of Health, Bethesda, MD, USA). The outlines of I4e and III4e targets were traced and the area was calculated in degree². Previous work has shown that both methods come to comparable conclusions,³¹ but to test comparability in our setting, one representative patient's visual field area (degree²) was calculated by using both methods. Only 1% difference in the calculated area (degree²) between the two methodologies was found and thus the results of the methodologies were deemed comparable in our setting.

Foveal Thickness. To assess foveal point thickness, all patients in both locations were scanned with spectral-domain optical coherence tomography (SD-OCT) using the Spectralis HRA+OCT platform (Heidelberg Engineering, Heidelberg, Germany) with its follow-up mode as described previously.³² Point measurement of retinal thickness in the central foveola was done with the caliper tool. This reports the thickness of the outer nuclear layer combined with the inner and outer segment length, that is, the photoreceptor layer, and has been shown to correlate with VA in patients with central serous chorioretinopathy.³³ Some evidence for a correlation between foveal point thickness and VA has also been reported for RP (Güven, et al. *IOVS* 2016;57:ARVO E-Abstract 0319). For SD-OCT, multiple high-speed B-scans were recorded to assess central retinal architecture and quantify thickness of the remaining neuroretinal tissue. To improve signal to noise ratio (SNR), $n \geq 9$ scans were averaged for each B-scan recording, whereby SNR improved by the square root of n . Foveal thickness (micrometers) was measured by using an in-built measurement tool of the Eye Explorer software (Heidelberg Engineering).

Electroretinography. Each patient's ERG measurements were assessed by using Espion (Diagnosys LLC, Lowell, MA, USA) following International Society for Clinical Electrophysiology of Vision (ISCEV) standards.³⁴ Amplitude values of dark-adapted (DA) 0.01 cd*s, DA 3.0 cd*s, DA 10.0 cd*s, and light-adapted (LA) 3.0 cd*s single flash recordings and 30-Hz flicker were extracted.

Statistical Analysis

Bivariate correlation, histograms, generalized linear mixed model analysis, and Kaplan-Meier survival curves were created by using Statistical Package for Social Sciences (SPSS) version 21 by IBM (SPSS, Inc., Chicago, IL, USA) for Windows.

Correlation Between Left and Right Eyes. Normality of target values distribution was assessed from the first measurement data of each patient by using superimposition of normal distribution line on histograms. Spearman's ρ analysis was performed to quantify the correlation between left and right eyes in nonnormally distributed values, using the first measurement of each patient.

Progression Rate Analysis. Owing to the large variety in both the number of follow-up measurements and the temporal spacing between repeated follow-up measurements, the progression rate was estimated by using generalized linear mixed model (GzLMM) analysis. Linear mixed models (LMMs) provide a framework for the analysis of longitudinal data with complex interactions and multilevel grouping of measurements and allow for the quantification of relationships between a continuous dependent variable and one or more predictor variables. Clustered data, such as left and right eyes of the same patients as well as repeated measurements, can be appropriately fitted, accounting for interactions due to data originating from the same subjects or groups. In contrast to repeated-measures analysis of variance, LMMs allow inclusion of more heterogeneous data, which makes it possible to include patients with an unequal number of repeated measurements in the analysis. GzLMMs add an additional layer of flexibility by allowing analysis of binary, ordinal, and count variables as well as nonlinear relationship functions.

In the following GzLMM, patient number was used as the subject. The number of “years since first visit” value was calculated for each repeated measure to account for temporal differences in measure repeats and was used in the model as “repeated measure” variable. The fixed effects were set to include the intercept and the “patient age at visit,” the latter specifying the age of the patient at the day of the follow-up measurement. The patient number was also used as a random effect. When left and right eyes were highly correlated, only the data from left eyes were used as target variable in order to simplify the model. Both linear model and gamma regression were assessed as link functions and the best-fitting mixed model was selected on the basis of the lowest information criteria values (Akaike corrected and Bayesian). When both link functions produced equal results, the model with more significant coefficients (lower *P* value) was preferred. Mixed model residuals distribution was assessed for normality as secondary measure of model suitability.

Vision Survival Analysis. Kaplan-Meier survival curve analysis was used to estimate cumulative survival of 6/6 vision, reading ability (defined as <6/15), and legal blindness (defined as <6/60) at different ages. Owing to wide variation in frequency of patient visits, all analyses were done by using both the complete set of patient visits as well as one visit per patient in order to avoid patients with many visits skewing the results. Both results are noted throughout the article.

RESULTS

Patient Cohort Characterization

The cohort was comprised of 50 male patients with a clinical and genetically confirmed diagnosis of XLRP3, ranging in age from 7 to 69 years. Between 1 and 17 visits were recorded per patient. Sixteen patients were seen only once, 34 patients were seen between 2 and 17 times. Of patients with a follow-up appointment, the average number of follow-up visits was 2.4 per patient (median = 1 visit). Follow-up time ranged from 2 to 72 months, with an average of 22 months in between visits (median = 14 months). Perimetry and ERG analysis were used to distinguish between the rod-cone phenotype, seen in most cases, and the much less frequent cone-rod phenotype.²¹ Forty-seven patients presented with a rod-cone phenotype, two with a cone-rod phenotype, and one patient showed a rod-cone phenotype with split fovea. The two patients presenting with a cone-rod phenotype had a deletion (c.2405_2406delAG; p.E802Gfs*32) and a nonsense mutation (c.2689G>T; p.E897*) in *ORF15*, while the patient with the

rod-cone phenotype with split fovea was hemizygous for c.3077_3080delAAGG; p.E1026Gfs*62. Though these numbers were not sufficient for a subgroup analysis, different phenotypes were color coded throughout analysis.

Eighteen percent of our patients were 20 years or younger, and of this cohort 44% were 10 years or younger at the age of onset. Of the nine patients who presented before the age of 20 years, five had mutations in exons 1–14 and four had *ORF15* mutations. Of patients who presented when younger than 10 years, three had a mutation in exons 1–14 and one had an *ORF15* mutation. None of these patients aged 20 years or younger were related and all were carriers of a different mutation.

Molecular Assessment

All patients were genetically analyzed, and mutations in *RPGR* were identified before this study (Fig. 1A; Table 1). The 50-patient *RPGR*-XLRP cohort comprised 41 different mutations, 19 of which were novel. Two mutations, c.2405_2406delAG and c.2236_2237delGA, occurred seven and four times, respectively. Even though both deletions occur within highly repetitive clusters of A and G repeats, the sequence following either deletion is not identical to the deleted repeats, making the alignment between the shifted nucleotides suboptimal.

Location of Mutations. Seventy-one percent of exonic mutations (i.e., excluding splice mutations and gross deletions) were present on exon *ORF15*, even though the number of *ORF15* nucleotides account for only 49% of the exonic *RPGR* sequence (Figs. 1B, 1C). In the present patient cohort, this clustering of mutations on *ORF15* was even more pronounced than previously noted.^{8,20} Missense mutations made up 20% of the total mutations and were clustered to the first half of the *RPGR* gene, with 80% occurring in exons 1 to 14, and only 20% in *ORF15* (Figs. 1B–D). Conversely, deletions, which represented by far the largest percentage of total mutations, occurred in the C-terminus of the exonic *RPGR* sequence in 85% of cases and were observed in the N-terminal half in only 15% of cases (Figs. 1B–D). This trend has been reported previously,^{35,36} with insertions, deletions (in/dels), and duplications clustered in the repetitive, purine (A/G)-rich regions of *ORF15*, and other substitutions, such as missense mutations, occurring predominantly in the first 14 exons of the gene.

Correlation of Location With Severity of Phenotype. To understand the impact of mutation location on phenotype, VA and perimetry (III4e target intensity) of patients with mutations in exons 1–14 were contrasted with VA and perimetry of patients with *ORF15* mutations. Data of right and left eye are dependent upon one another, so use of both right and left eye data points might have skewed the data distribution. Since analysis showed high symmetry between both eyes for VA and perimetry, only the right eye data set was used. Analysis was done by using one visit per patient. Significant variability, but no significant difference, in VA or perimetry could be shown between mutations located in exons 1–14 and mutations on *ORF15* (VA *p* = 0.90, perimetry *P* = 0.58) (Supplementary Fig. S1). These results were confirmed by the analysis of a selected age group (30–40 years) to control for difference in progression as a potential confounder. Since the two patients with cone-rod phenotypes were not shown to be outliers in disease progression (Fig. 3), they were included in the before mentioned analysis (see below).

Analysis of Disease Symmetry Between Eyes

The functional endpoint foveal thickness indicated the least robust degree of symmetry ($\rho = 0.75$, $n = 35$, $P < 0.001$). In contrast, the effect of degeneration on central visual function was highly symmetrical between right and left eye ($\rho = 0.85$, n

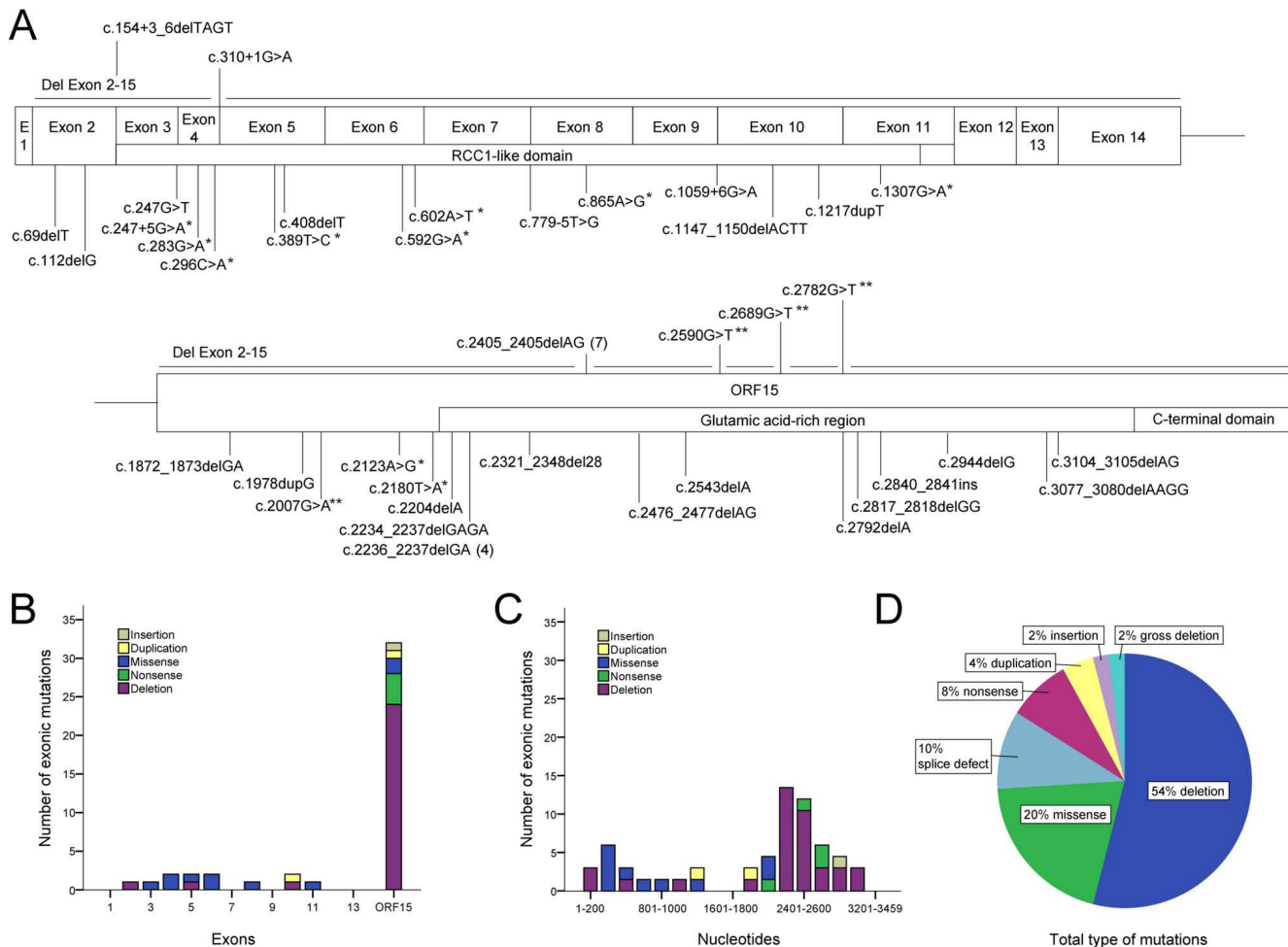


FIGURE 1. Overview of *RPGR* mutations showing mutation location and frequency as well as types of mutations occurring in a 50-patient *RPGR*-XLRP cohort. (A) Bar graph shows that *ORF15*, the terminal exon of *RPGR*, takes up almost half of the exonic *RPGR* sequence. Overview by exons (B) shows that 31 mutations (71%) cluster on the purine-rich, repetitive C-terminal exon *ORF15*. Overview by cDNA nucleotide position (C) shows that 8 of 10 missense mutations (80%) cluster on exons 1–14, whereas 23 of 27 deletions (85%) occur in *ORF15*. (D) Deletions were the most frequent type of mutation found in this patient cohort (54%), followed by missense mutations (20%). Splice defects and nonsense mutations occurred with roughly equal frequency, 10% and 8%, respectively. Duplications were present in 4% of patients, insertions as well as gross deletions occurred in 2% of patients. *Missense mutation. **Nonsense mutation.

= 50, $P < 0.001$; Fig. 2A). Perimetry showed an even higher degree of symmetry using isopter III4e ($\rho = 0.96$, $n = 38$, $P < 0.001$, Fig. 2C). Correlation of isopter I4e values was even higher ($\rho = 0.97$, $n = 30$, $P < 0.001$), yet likely represents an overestimation, as 40% of I4e measurements were (close to) zero in both eyes, hence creating a floor effect. As objective measure of retinal function, ERG b-wave amplitudes were symmetrical overall, with the highest symmetry without confounding floor effect found in DA single-flash responses following a 3 cd/s stimulus ($\rho = 0.98$, $n = 32$, $P < 0.001$; Fig. 2D) and in 30-Hz flicker (Spearman's $\rho = 0.95$, $n = 32$, $P < 0.001$). Noteworthy, patients with cone-rod or rod-cone phenotype with split fovea did not present as outliers in symmetry analysis.

Analysis of Disease Progression

When analyzing the same structural and functional endpoints regarding their value in assessing disease progression, VA (Fig. 3A) and foveal thickness (Fig. 3B) proved to be the most useful parameters. Their relationship to age is best described by a natural logarithmic function, with logarithmic progression rates as reported in Table 2. Assessing disease progression by

perimetry (isopter III4e) only makes sense within the first two decades of life, as the progressive visual field loss is (near-)complete as early as age 20 to 25 years (Fig. 3C; Supplementary Table S1). This creates a floor effect and results in limited discriminatory power for any efficacy analysis. ERG data (Fig. 3D; Supplementary Table S1) show no correlation with age. Again, patients with cone-rod phenotype or rod-cone phenotype with split fovea did not present as outliers in disease progression regardless of the outcome measure.

Subgroup Analysis of Disease Progression

To determine whether a homogenous disease progression in patients with the same mutations could be shown, two subgroups of patients carrying the same mutation were analyzed.

***RPGR* Mutation c.2405_2406delAG.** The first subgroup comprised seven patients carrying the c.2204_2205delAG; p.E802Gfs*32 mutation (Supplementary Fig. S2). Patient No. 49 and patient No. 50 were second-degree relatives. Despite the identical mutation, no correlation of disease progression with age could be shown. The variability was further underscored

TABLE 1. Overview of Molecular Testing Results in *RPGR*-XLRP Patient Cohort

Patient No.	Hemizygous Mutations in <i>RPGR</i>			Mutation Type	Previously Described
	Nucleotide Level	Exon	Protein Level		
3	Gross deletion spanning exons 2-15 (length of deletion not defined)	2		Gross deletion	Novel
12	c.69delT	2	p.E24Kfs*44	Deletion	Novel
15	c.112delG	2	p.V38Yfs*30	Deletion	Novel
29	c.154+3_6delTAGT			Splice defect	Neidhardt et al. ⁵² 2008
8	c.247G>T	3	p.A83S	Missense	Glöckle et al. ²⁷ 2014
26	c.247+5G>A			Splice defect	Novel
25	c.283G>A	4	p.G95R	Missense	Novel
17	c.296C>A	4	p.T99N	Missense	Miano et al. ⁴⁹ 1999
38	c.310+1G>A			Splice defect	Sharon et al. ⁶ 2003
16	c.389T>C	5	p.F130S	Missense	Novel
42	c.408delT	5	p.F136L	Deletion	Shu et al. ³⁵ 2007
19	c.592G>A	6	p.G198R	Missense	Sharon et al. ⁶ 2015
6	c.602A>T	6	p.H201L	Missense	Novel*
43	c.779-5T>G			Splice defect	Neidhardt et al. ⁵² 2008
39	c.865A>G	8	p.I289V	Missense	Miano et al. ⁴⁹ 1999
37	c.1059+6G>A			Splice defect	Novel
41	c.1147_1150delACTT	10	p.T383Afs*13	Deletion	Novel
28	c.1217dupT	10	p.S407Ifs*46	Duplication	Novel
46	c.1307G>A	11	p.G436D	Missense	Sharon et al. ⁶ 2000
1	c.1872_1873delGA	15	p.E624Dfs*5	Deletion	Pusch et al. ²⁰ 2002
22	c.1978dupG	15	p.Glu660Glyfs*4	Duplication	Novel
31	c.2007G>A	15	p.W669*	Nonsense	Bader et al. ⁵ 2003
9	c.2123A>G	15	p.E708G	Missense	Novel
21	c.2180T>A	15	p.M727K	Missense	Novel
24	c.2234_2237delGAGA	15	p.R745Kfs*69	Deletion	Breuer et al. ⁵⁰ 2002
7	c.2236_2237delGA	15	p.E746Rfs*23	Deletion	Vervoort et al. ⁸ 2000
10	c.2236_2237delGA	15	p.E746Rfs*23	Deletion	Vervoort et al. ⁸ 2000
23	c.2236_2237delGA	15	p.E746Rfs*23	Deletion	Vervoort et al. ⁸ 2000
48	c.2236_2237delGA	15	p.E746Rfs*23	Deletion	Vervoort et al. ⁸ 2000
30	c.2321_2348del28	15	p.E774Gfs*32	Deletion	Novel
14	c.2384delA	15	p.E795Gfs*20	Deletion	Pusch et al. ²⁰ 2002
11	c.2405_2406delAG	15	p.E802Gfs*32	Deletion	Vervoort et al. ⁸ 2000†
32	c.2405_2406delAG	15	p.E802Gfs*32	Deletion	Vervoort et al. ⁸ 2000
33	c.2405_2406delAG	15	p.E802Gfs*32	Deletion	Vervoort et al. ⁸ 2000
44	c.2405_2406delAG	15	p.E802Gfs*32	Deletion	Vervoort et al. ⁸ 2000
45	c.2405_2406delAG	15	p.E802Gfs*32	Deletion	Vervoort et al. ⁸ 2000
49	c.2405_2406delAG	15	p.E802Gfs*32	Deletion	Vervoort et al. ⁸ 2000‡
50	c.2405_2406delAG	15	p.E802Gfs*32	Deletion	Vervoort et al. ⁸ 2000§
35	c.2476_2477delAG	15	p.R826Gfs*8	Deletion	Pusch et al. ²⁰ 2002
27	c.2543delA	15	p.E848Gfs*241	Deletion	Pusch et al. ²⁰ 2002
40	c.2590G>T	15	p.E864*	Nonsense	Pusch et al. ²⁰ 2002
5	c.2689G>T	15	p.E897*	Nonsense	Glöckle et al. ²⁷ 2014†
34	c.2782G>T	15	p.G928*	Nonsense	Pusch et al. ²⁰ 2002
47	c.2790_2791delGG	15	p.E931Gfs*147	Deletion	Shu et al. ³⁵ 2007
36	c.2792delA	15	p.E931Gfs*158	Deletion	Pelletier et al. ⁵¹ 2007
13	c.2840_2841ins (length of insertion not defined)	15		Insertion	Novel
20	c.2944delG	15	p.E982Kfs*107	Deletion	Sharon et al. ⁶ 2003
2	c.2997_2998delGG	15	p.E1000Gfs*78	Deletion	Pusch et al. ²⁰ 2002
18	c.3077_3080delAAGG	15	p.E1026Gfs*62	Deletion	Novel
4	c.3104_3105delAG	15	p.E1035Gfs*43	Deletion	Novel

The 50-patient cohort exhibited 41 different mutations in the *RPGR* gene (NM_001034853). Two mutations, c.2405_2406delAG and c.2236_2237delGA, appeared more frequently, seven and four times, respectively. Two patients are second-degree relatives. RefSeq NM_001034853, NP_001030025.

* Variant of unclear pathogenicity.

† Cone-rod dystrophy.

‡ Uncle of patient No. 50.

§ Nephew of patient No. 49.

by the cone-rod phenotype of patient No. 11, whereas the other six patients exhibited a rod-cone phenotype.

***RPGR* Mutation c.2236_2237delGA.** The second subgroup comprises four patients with the c.2236_2237delGA,

p.E746Rfs*23 mutation (Supplementary Fig. S3). In contrast to the c.2405_2405delAG mutation, c.2236_2237delGA showed a homogenous disease progression when looking at VA ($R^2 = 0.58$, $n = 4$, $P = 0.11$) and foveal thickness ($R^2 = 0.96$, $n = 4$, $P =$

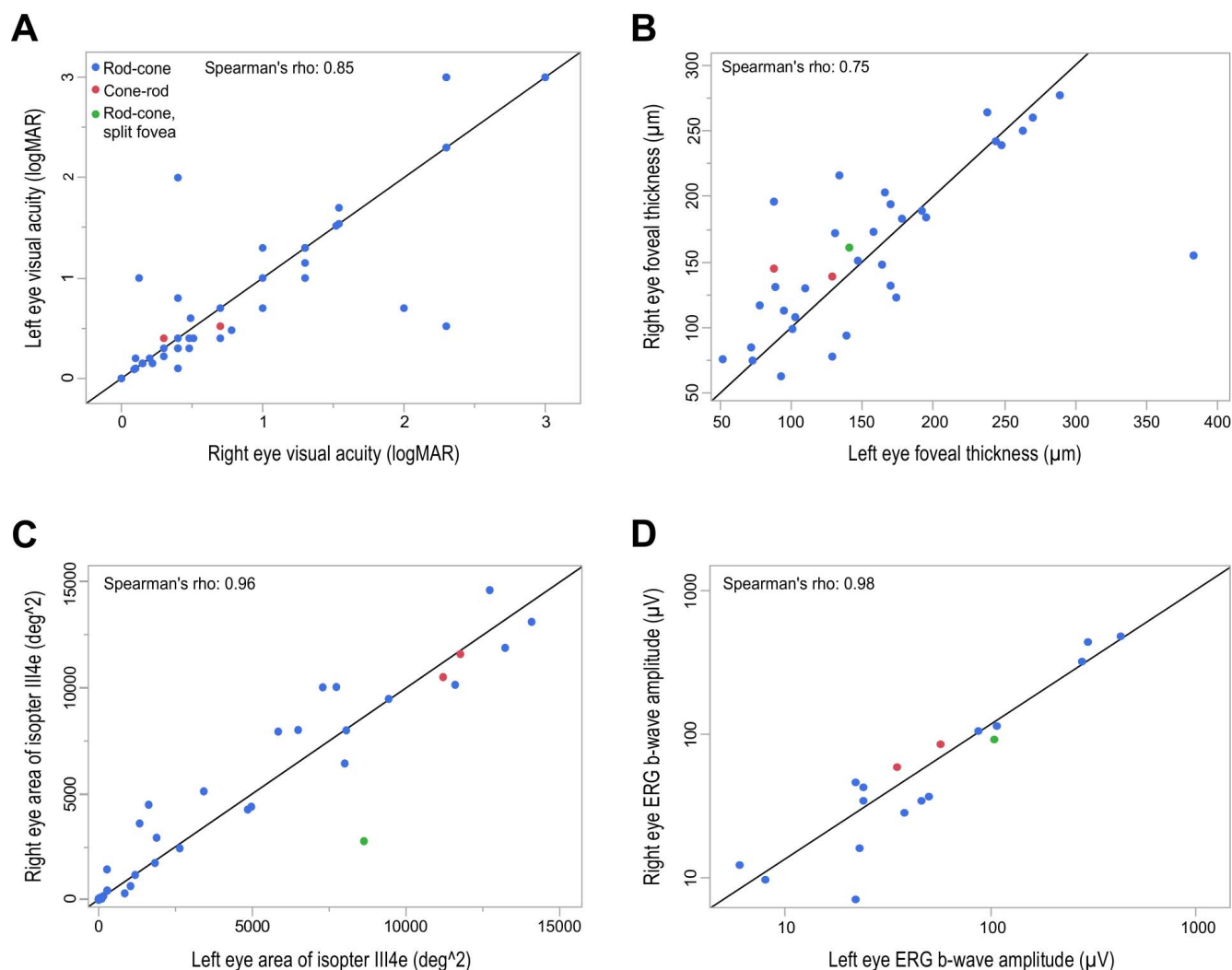


FIGURE 2. Symmetry analysis between right and left eyes using VA, foveal thickness, III4e target perimetry, and DA 3.0 cd*s b-wave amplitude as outcome measures. Degeneration and its effect on central visual function (A) was fairly symmetrical between right and left eyes (Spearman's $\rho = 0.85$). Foveal thickness (B) was fairly symmetrical (Spearman's $\rho = 0.75$). Kinetic perimetry using III4e target (C) showed very good symmetry between eyes (Spearman's $\rho = 0.96$). ERG b-wave amplitude elicited by DA 3.0 cd*s flash (D) showed a very good symmetry (Spearman's $\rho = 0.98$) as well.

0.05). ERG endpoints exhibited ρ values ranging from 0.50 (DA 3.0 cd*s) to 0.81 (LA 3.0 cd*s). R^2 for 30-Hz flicker was 0.79 ($n = 4$, $P < 0.01$). In perimetry, neither target (I4e or III4e) showed a homogenous disease progression. This is the result of patient No. 48 being an outlier in the I4e target perimetry (III4e not available), and patient No. 7 showing a relatively well-preserved III4e target perimetry.

Kaplan-Meier Survival Curve

Loss of VA is perhaps the most relevant outcome measure for patients. To estimate the decline of VA despite large phenotypic variability between patients, a Kaplan-Meier survival curve was calculated (Fig. 4) by using three cutoff points: loss of 6/6 vision (0.0 logMAR), loss of reading ability (0.4 logMAR), and a drop of vision under the limit for legal blindness (1.0 logMAR). Data from right and left eyes were calculated separately and again showed high degree of symmetry.

The most severe loss of VA was predicted to occur in the third and fourth decade of life. At age 20 years, over 80% of patients retained 6/6 vision and over 90% of patients were

predicted to retain their ability to read. By age 40 years over 20% of patients were anticipated to be legally blind, with over 50% predicted to have lost their ability to read, and only 30% to retain 6/6 vision. In general, the mean estimated survival time for 6/6 vision was 34 years (± 2.9 ; 95% confidence interval), with a loss of reading ability occurring at 39 years (± 2.6) and reaching the limit for legal blindness at 48 (± 1.6) years.

DISCUSSION

The severity of XLRP due to *RPGR* mutations is evident in the early onset, with patients presenting as early as 7 years of age and nine patients presenting before the age of 20 years. Of the four patients who presented while under the age of 10 years, three had mutations in exons 1–14, which might hint at a trend of mutations in exons 1–14 presenting at a younger age, but the statistical power is not reliable owing to the small sample size.

ORF15 was confirmed as a sequence particularly vulnerable for mutation in *RPGR*, with 73% of mutations occurring in this terminal exon. However, *ORF15* mutations did not demon-

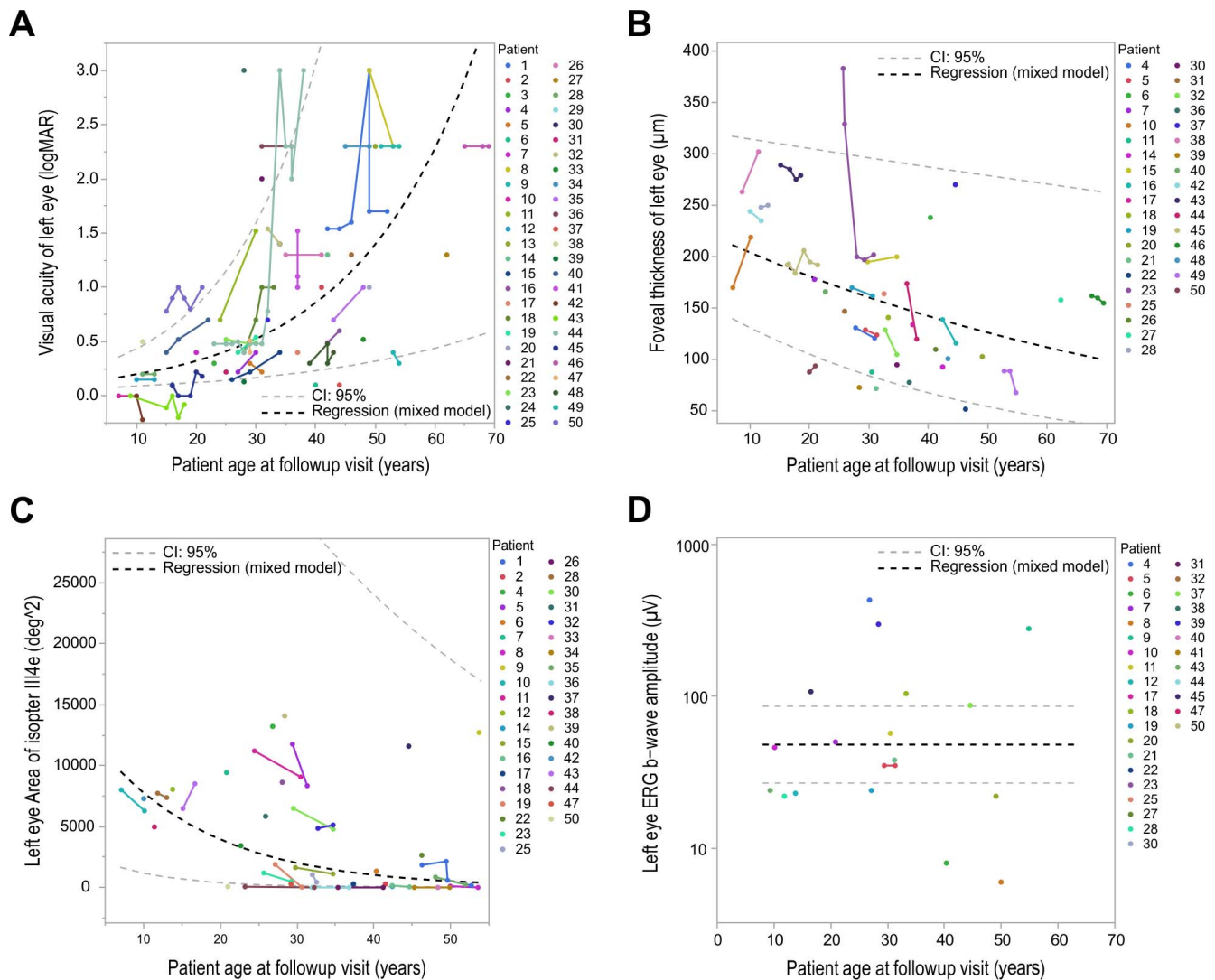


FIGURE 3. Progression analysis of *RPGR*-XLRP patients using left-eye VA, foveal thickness, III4e target perimetry, and DA 3.0 cd*s ERG: Plotting of left-eye VA (A) and foveal thickness (B) against age shows a logarithmic correlation function expressing a relationship between the age and outcome measure. Epiretinal membrane formation resulted in increased foveal thickness in single patients. These were not excluded, since inclusion/exclusion did not generally change the outcome of analysis. The logarithmic function was also best suited to describe the relationship between kinetic perimetry and age (C) or between DA 3.0 cd*s b-wave amplitude and age (D).

strate a different degree of severity or phenotypic pattern (rod-cone versus cone-rod dystrophy) than mutations occurring in exons 1–14. These results differ from those of Sharon et al.⁶ and Fahim et al.²² who have demonstrated a milder disease phenotype in patients with *ORF15* mutations than in patients with mutations in the N-terminal RCC1-like domain. It has been

speculated that such a genotype/phenotype correlation could be explained by residual function of the truncated protein, since nonsense mutations in the terminal exon (*ORF15*) are not expected to undergo nonsense-mediated mRNA decay.^{6,37} On the other hand, Hong et al.³⁸ have shown a gain-of-function mutation in *ORF15* that causes more severe disease progres-

TABLE 2. Average Disease Progression Rate per Age Group

Age Group, Range, y	Estimated Average Yearly Progression Rate (CI: 95%)			
	Visual Acuity, logMAR/y	Foveal Thickness, $\mu\text{m}/\text{y}$	Perimetry III4e, deg^2/y	ERG b3.SF, $\mu\text{V}/\text{y}$
7–20	0.01 (0, 0.04)	–2.35 (–2.67, –0.93)	–416.44 (–88.83, –1165.17)	0 (0, 0)
21–40	0.03 (0.01, 0.11)	–1.91 (–1.84, –0.89)	–131.07 (–13.23, –761.75)	0 (0, 0)
41–60	0.07 (0.01, 0.39)	–1.51 (–1.18, –0.83)	–33.64 (–1.41, –462.03)	0 (0, 0)

Average yearly progression rates for VA, foveal thickness, perimetry (III4e), and ERG (b3.SF) were based on GzLMM results (Supplementary Table S1). VA loss appeared to be the slowest in the younger patients with increased progression rates and interpatient variability in older patients. Whereas foveal thickness and perimetry loss progression rates were highest in the younger age groups and slowed down with age, ERG progression did not appear to be correlated with age. CI, confidence interval.

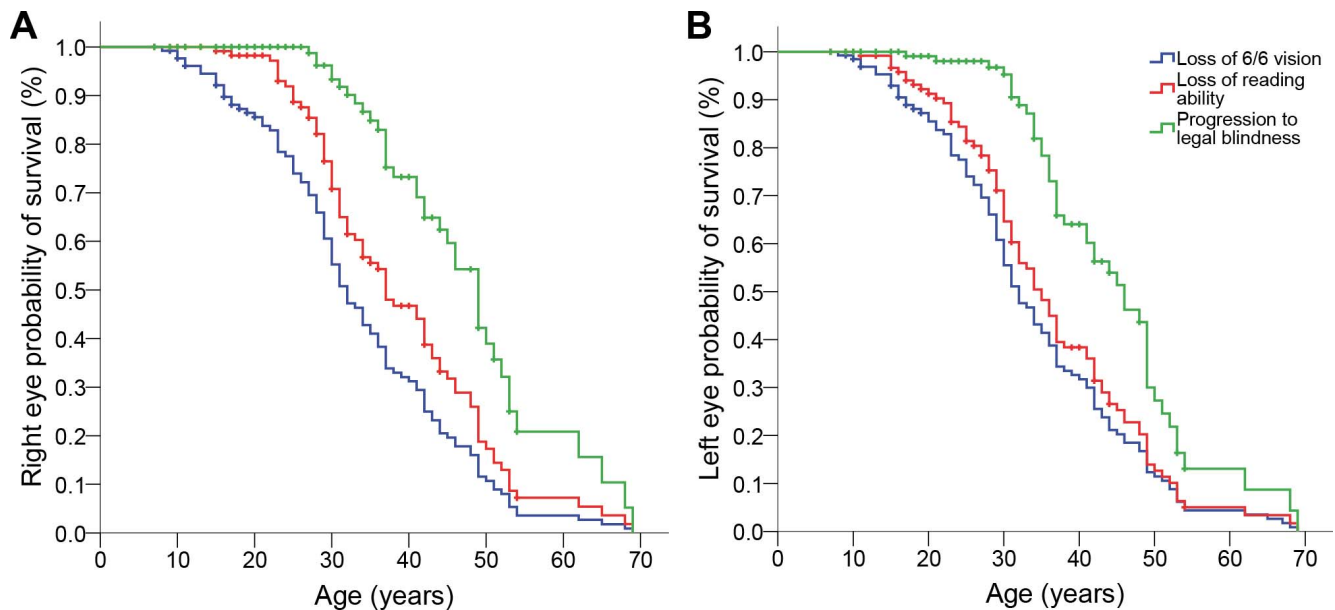


FIGURE 4. Kaplan-Meier survival curves (KMCs) for *RPGR*-XLRP patients. KMC for right eyes (A) predicted a loss of 6/6 vision at a mean age of 34 years (± 2.9 ; 95% confidence interval), a loss of reading ability at 39 years (± 2.6), and progression to legal blindness at 48 years (± 1.6). KMCs for left eyes (B) were similar, estimating a loss of 6/6 vision at a mean of 34 years (± 2.4), a loss of reading ability at 37 years (± 2.5), and a reaching of the legal limit for legal blindness at 45 years (± 3.1).

sion than a *null* mutation. Additionally, dogs with X-linked progressive retinal atrophy (XLPRA), the canine homologue to XLRP3 in humans, show either a slow (XLPRA1) or more severe (XLPRA2) disease progression, although both feature deletions in *ORF15* within 52 nucleotides from another.^{37,39} This is in line with our observations in this study, where no strict genotype/phenotype correlation became apparent.

Massof et al.,⁴⁰ who have analyzed VA and perimetry (V4e) of 60 genetically unclassified RP patients, report a high rate of bilateral symmetry in their probably genetically heterogeneous patient cohort. Of the patients who were diagnosed by clinical phenotype alone, a mere 4% show an X-linked inheritance pattern. Findings of the current study add the important observation that the assumption of symmetry holds true for XLRP patients with mutations in *RPGR*. In future therapeutic interventional trials using monocular treatment, the fellow eye can therefore be used as an internal control. Examples of this practice can be found in phase 1 and 2 trials conducted on Leber congenital amaurosis patients.^{41,42} In other instances, regulatory agencies prefer the use of an interindividual control, despite bilateral symmetry of disease.⁴³ The assumption of bilateral symmetry holds true not only for VA and perimetry, but also for foveal thickness and ERG b-wave amplitudes. In particular, perimetry with the isopter area of III4e displayed excellent symmetry. However, its utility as an efficacy endpoint in an interventional trial is limited by the early loss of visual field, which would make it hard to prove that there is lack of progression in adult patients.

Considering both symmetry and progression rate, VA might be the best choice as functional outcome measure to estimate treatment efficacy. According to our data, VA is less variable in younger patients. However, we did not assess test-retest variability in this retrospective study and this would have to be assessed in a prospective trial. However, the psychophysical nature of VA or perimetry may be seen critically in an unmasked trial. Bittner et al.⁴⁴ have shown that test-retest variability could be limited to <20% in perimetry, but not further, by using a single experienced operator. ERG on the other hand offers an objective, quantitative outcome measure

that also displays very good symmetry. Yet, our analysis showed no significant correlation between ERG values and disease progression. A limitation of full-field ERG is that it is a sum potential and—in contrast to perimetry—does not feature a spatial resolution. Multifocal ERG was not analyzed in this study owing to lack of appropriate data in this retrospective, cross-sectional study over two national sites. A prospective trial using the outcome measures multifocal ERG, VA, perimetry, and OCT would be beneficial to further compare the advantages of each outcome measure. Specifically, the width of the photoreceptor ellipsoid zone (EZ), as identified in OCT, is another potentially highly relevant outcome measure for disease progression in XLRP3.^{45–47} Birch et al.⁴⁵ have demonstrated that loss of EZ width at the transitional zone between healthy and diseased retina correlates to loss of visual field in XLRP patients. EZ width has a low repeat variability, is not subject to floor effects in the assessment of disease progression, and is an anatomic measure that reflects the functional outcome of field sensitivity.

As subgroup analysis shows, a uniform disease progression or phenotype cannot be guaranteed even in patients carrying the same mutation. The conflicting evidence on variability in cohorts carrying the same mutation may be due to low statistical power of small cohorts and/or to unknown genetic modifiers and environmental circumstances influencing disease progression. Fahim et al.²² have found two SNPs that are associated with variable severity of retinal genetic disease.²² A continued search for potential genetic modifiers might help explain variability of genotype-phenotype relationship and eventually help to predict prognosis for individual patients. Since disease progression between patients can differ so greatly from each other, an interindividual control cannot be reliable. This again emphasizes the value of an intraindividual control in the form of the contralateral eye in an interventional trial, given of course, that the intervention is not applied systemically.

Kaplan-Meier survival curves showed the most prominent decline in VA throughout the third and fourth decade of life. The median age to reach legal blindness in our patient cohort

was compatible with the results of Sandberg et al.⁴ who calculate a median survival age of 45 years for XLRP3 patients. In a clinical trial in which efficacy is defined as lack of progression, patients should be selected before or at the beginning of this rapid rate of decline. On the other hand, a clinical trial designed to show efficacy in form of VA gain might need to choose patients toward the end or after the period of sharp decline. Beltran et al.⁴⁸ recently have shown in a canine dog model of XLRP3 that treatment during intermediate stage of disease is able to substantially and significantly slow and arrest the progression of disease, a finding that potentially broadens the therapeutic window of intervention in patients with XLRP3.

In summary, our results indicated that degeneration between eyes is symmetrical, and therefore the contralateral eye can be used as an internal control in an interventional trial. Sensitivity was the greatest when using VA and foveal thickness as outcome measures. Perimetry with III4e may be a useful endpoint in younger patients with less advanced stage of disease. Even individual mutations showed variability in disease progression and presenting phenotype (rod-cone versus cone-rod). Contrary to previous analysis,⁶ mutation location in or outside of *ORF15* could not be correlated with severity of phenotype. Kaplan-Meier analysis showed the strongest decline in VA during the third and fourth decade of life. The median age for patients to reach legal blindness was 48 years. A prospective observational trial of genetically confirmed XLRP3 patients, using standardized outcome measures such as perimetry, multifocal ERG, OCT, and VA, would be needed to further explore the utility of these endpoints for efficacy studies.

Acknowledgments

The authors thank Aline Naumann from the Institute of Clinical Epidemiology and Applied Biometrics and Philipp Berens from the Neural Data Science for Vision Research Lab for their advice on the statistics, and Karl Ulrich Bartz-Schmidt and Marius Ueffing for their supporting role in this research.

Supported by Gesellschaft zur Förderung der Neuroophthalmologie e.V. (IPS, J-SB), Tistou & Charlotte Kerstan Foundation (MDF), Pro Retina e.V. (J-SB, IPS, MDF), UK Medical Research Council (MR/K003690/1) (MDF); and NIHR Oxford Biomedical Research Centre (REM, SMD).

Disclosure: **J.-S. Bellingrath**, None; **G.A. Ochakovski**, None; **I.P. Seitz**, None; **S. Kohl**, None; **E. Zrenner**, None; **N. Hanig**, None; **H. Prokisch**, None; **B.H. Weber**, None; **S.M. Downes**, None; **S. Ramsden**, None; **R.E. MacLaren**, NightstaRx Ltd. (C, F), University of Oxford (R), P; **M.D. Fischer**, NightstaRx Ltd. (C, F, S), EyeServ GmbH (C), University of Oxford (R), P

References

- Pawlyk BS, Bulgakov OV, Sun X, et al. Photoreceptor rescue by an abbreviated human RPGR gene in a murine model of X-linked retinitis pigmentosa. *Gene Ther.* 2016;23:196–204.
- Wright AF, Chakarova CF, Abd El-Aziz MM, Bhattacharya SS. Photoreceptor degeneration: genetic and mechanistic dissection of a complex trait. *Nat Rev Genet.* 2010;11:273–284.
- Hartong DT, Berson EL, Dryja TP. Retinitis pigmentosa. *Lancet.* 2006;368:1795–1809.
- Sandberg MA, Rosner B, Weigel-DiFranco C, Dryja TP, Berson EL. Disease course of patients with X-linked retinitis pigmentosa due to RPGR gene mutations. *Invest Ophthalmol Vis Sci.* 2007;48:1298–1304.
- Bader I, Brandau O, Achatz H, et al. X-linked retinitis pigmentosa: RPGR mutations in most families with definite X linkage and clustering of mutations in a short sequence

- stretch of exon ORF15. *Invest Ophthalmol Vis Sci.* 2003;44:1458–1463.
- Sharon D, Sandberg MA, Rabe VW, Stillberger M, Dryja TP, Berson EL. RP2 and RPGR mutations and clinical correlations in patients with X-linked retinitis pigmentosa. *Am J Hum Genet.* 2003;73:1131–1146.
- Meindl A, Dry K, Herrmann K, et al. A gene (RPGR) with homology to the RCC1 guanine nucleotide exchange factor is mutated in X-linked retinitis pigmentosa (RP3). *Nat Genet.* 1996;13:35–42.
- Vervoort R, Lennon A, Bird AC, et al. Mutational hot spot within a new RPGR exon in X-linked retinitis pigmentosa. *Nat Genet.* 2000;25:462–466.
- Roepman R, van Duijnhoven G, Rosenberg T, et al. Positional cloning of the gene for X-linked retinitis pigmentosa 3: homology with the guanine-nucleotide-exchange factor RCC1. *Hum Mol Genet.* 1996;5:1035–1041.
- Kirschner R, Rosenberg T, Schultz-Heienbrok R, et al. RPGR transcription studies in mouse and human tissues reveal a retina-specific isoform that is disrupted in a patient with X-linked retinitis pigmentosa. *Hum Mol Genet.* 1999;8:1571–1578.
- Roepman R, Bernoud-Hubac N, Schick DE, et al. The retinitis pigmentosa GTPase regulator (RPGR) interacts with novel transport-like proteins in the outer segments of rod photoreceptors. *Hum Mol Genet.* 2000;9:2095–2105.
- Neidhardt J, Glaus E, Barthelmes D, Zeitz C, Fleischhauer J, Berger W. Identification and characterization of a novel RPGR isoform in human retina. *Hum Mutat.* 2007;28:797–807.
- Schmid F, Glaus E, Cremers FP, Klockener-Gruissem B, Berger W, Neidhardt J. Mutation- and tissue-specific alterations of RPGR transcripts. *Invest Ophthalmol Vis Sci.* 2010;51:1628–1635.
- Hong DH, Pawlyk B, Sokolov M, et al. RPGR isoforms in photoreceptor connecting cilia and the transitional zone of motile cilia. *Invest Ophthalmol Vis Sci.* 2003;44:2413–2421.
- Mavlyutov TA, Zhao H, Ferreira PA. Species-specific subcellular localization of RPGR and RPGRIP isoforms: implications for the phenotypic variability of congenital retinopathies among species. *Hum Mol Genet.* 2002;11:1899–1907.
- Patil H, Guraju MR, Cho KI, et al. Structural and functional plasticity of subcellular tethering, targeting and processing of RPGRIP1 by RPGR isoforms. *Biol Open.* 2012;1:140–160.
- Iannaccone A, Breuer DK, Wang XF, et al. Clinical and immunohistochemical evidence for an X linked retinitis pigmentosa syndrome with recurrent infections and hearing loss in association with an RPGR mutation. *J Med Genet.* 2003;40:e118.
- Hong DH, Yue G, Adamian M, Li T. Retinitis pigmentosa GTPase regulator (RPGR)-interacting protein is stably associated with the photoreceptor ciliary axoneme and anchors RPGR to the connecting cilium. *J Biol Chem.* 2001;276:12091–12099.
- Boylan JP, Wright AF. Identification of a novel protein interacting with RPGR. *Hum Mol Genet.* 2000;9:2085–2093.
- Pusch CM, Broghammer M, Jurklics B, Besch D, Jacobi FK. Ten novel ORF15 mutations confirm mutational hot spot in the RPGR gene in European patients with X-linked retinitis pigmentosa. *Hum Mutat.* 2002;20:405.
- Zahid S, Khan N, Branham K, et al. Phenotypic conservation in patients with X-linked retinitis pigmentosa caused by RPGR mutations. *JAMA Ophthalmol.* 2013;131:1016–1025.
- Fahim AT, Bowne SJ, Sullivan LS, et al. Allelic heterogeneity and genetic modifier loci contribute to clinical variation in males with X-linked retinitis pigmentosa due to RPGR mutations. *PLoS One.* 2011;6:e23021.
- Walia S, Fishman GA, Swaroop A, et al. Discordant phenotypes in fraternal twins having an identical mutation in exon

- ORF15 of the RPGR gene. *Arch Ophthalmol*. 2008;126:379-384.
24. Beltran WA, Cideciyan AV, Lewin AS, et al. Gene therapy rescues photoreceptor blindness in dogs and paves the way for treating human X-linked retinitis pigmentosa. *Proc Natl Acad Sci U S A*. 2012;109:2132-2137.
 25. Deng WT, Dyka FM, Dinculescu A, et al. Stability and safety of an AAV vector for treating RPGR-ORF15 X-linked retinitis pigmentosa. *Hum Gene Ther*. 2015;26:593-602.
 26. Wu Z, Hiriyan S, Qian H, et al. A long-term efficacy study of gene replacement therapy for RPGR-associated retinal degeneration. *Hum Mol Genet*. 2015;24:3956-3970.
 27. Glöckle N, Kohl S, Mohr J, et al. Panel-based next generation sequencing as a reliable and efficient technique to detect mutations in unselected patients with retinal dystrophies. *Eur J Hum Genet*. 2014;22:99-104.
 28. Holladay JT. Proper method for calculating average visual acuity. *J Refract Surg*. 1997;13:388-391.
 29. Fischer MD, Fleischhauer JC, Gillies MC, Sutter FK, Helbig H, Barthelmes D. A new method to monitor visual field defects caused by photoreceptor degeneration by quantitative optical coherence tomography. *Invest Ophthalmol Vis Sci*. 2008;49:3617-3621.
 30. Wiethoff S, Zhou A, Schols L, Fischer MD. Retinal nerve fibre layer loss in hereditary spastic paraplegias is restricted to complex phenotypes. *BMC Neurol*. 2012;12:143.
 31. Rowe FJ, Rowlands A. Comparison of diagnostic accuracy between Octopus 900 and Goldmann kinetic visual fields. *BioMed Res Int*. 2014;2014:11.
 32. Fischer MD, Willmann G, Schatz A, et al. Structural and functional changes of the human macula during acute exposure to high altitude. *PLoS One*. 2012;7:e36155.
 33. Matsumoto H, Sato T, Kishi S. Outer nuclear layer thickness at the fovea determines visual outcomes in resolved central serous chorioretinopathy. *Am J Ophthalmol*. 2009;148:105-110.e101.
 34. McCulloch DL, Marmor MF, Brigell MG, et al. ISCEV Standard for full-field clinical electroretinography (2015 update). *Doc Ophthalmol*. 2015;130:1-12.
 35. Shu X, Black GC, Rice JM, et al. RPGR mutation analysis and disease: an update. *Hum Mutat*. 2007;28:322-328.
 36. Wright AF, Shu X. Focus on molecules: RPGR. *Exp Eye Res*. 2007;85:1-2.
 37. Zhang Q, Acland GM, Wu WX, et al. Different RPGR exon ORF15 mutations in Canids provide insights into photoreceptor cell degeneration. *Hum Mol Genet*. 2002;11:993-1003.
 38. Hong DH, Pawlyk BS, Adamian M, Li T. Dominant, gain-of-function mutant produced by truncation of RPGR. *Invest Ophthalmol Vis Sci*. 2004;45:36-41.
 39. Zeiss CJ, Acland GM, Aguirre GD. Retinal pathology of canine X-linked progressive retinal atrophy, the locus homologue of RP3. *Invest Ophthalmol Vis Sci*. 1999;40:3292-3304.
 40. Massof RW, Finkelstein D, Starr SJ, Kenyon KR, Fleischman JA, Maumenee IH. Bilateral symmetry of vision disorders in typical retinitis pigmentosa. *Br J Ophthalmol*. 1979;63:90-96.
 41. Jacobson SG, Cideciyan AV, Roman AJ, et al. Improvement and decline in vision with gene therapy in childhood blindness. *N Engl J Med*. 2015;372:1920-1926.
 42. Bainbridge JW, Mehat MS, Sundaram V, et al. Long-term effect of gene therapy on Leber's congenital amaurosis. *N Engl J Med*. 2015;372:1887-1897.
 43. Birch DG, Weleber RG, Duncan JL, Jaffe GJ, Tao W. Ciliary Neurotrophic Factor Retinitis Pigmentosa Study Groups. Randomized trial of ciliary neurotrophic factor delivered by encapsulated cell intraocular implants for retinitis pigmentosa. *Am J Ophthalmol*. 2013;156:283-292.e1.
 44. Bittner AK, Iftikhar MH, Dagnelie G. Test-retest, within-visit variability of Goldmann visual fields in retinitis pigmentosa. *Invest Ophthalmol Vis Sci*. 2011;52:8042-8046.
 45. Birch DG, Locke KG, Felius J, et al. Rates of decline in regions of the visual field defined by frequency-domain optical coherence tomography in patients with RPGR-mediated X-linked retinitis pigmentosa. *Ophthalmology*. 2015;122:833-839.
 46. Birch DG, Locke KG, Wen Y, Locke KI, Hoffman DR, Hood DC. Spectral-domain optical coherence tomography measures of outer segment layer progression in patients with X-linked retinitis pigmentosa. *JAMA Ophthalmol*. 2013;131:1143-1150.
 47. Tee JJ, Carroll J, Webster AR, Michaelides M. Quantitative analysis of retinal structure using spectral domain optical coherence tomography in RPGR-associated retinopathy. *Am J Ophthalmol*. 2017;178:18-26.
 48. Beltran WA, Cideciyan AV, Iwabe S, et al. Successful arrest of photoreceptor and vision loss expands the therapeutic window of retinal gene therapy to later stages of disease. *Proc Natl Acad Sci U S A*. 2015;112:E5844-E5853.
 49. Miano MG, Testa F, Strazzullo M, et al. Mutation analysis of the RPGR gene reveals novel mutations in south European patients with X-linked retinitis pigmentosa. *Eur J Hum Genet*. 1999;7:687-694.
 50. Breuer DK, Yashar BM, Fillippova E, et al. A comprehensive mutation analysis of RP2 and RPGR in North American cohort of families with X-linked retinitis pigmentosa. *Am J Hum Genet*. 2002;70:1545-1554.
 51. Pelletier V, Jambou M, Delphin N, et al. Comprehensive survey of mutations in RP2 and RPGR in patients affected with distinct retinal dystrophies: genotype-phenotype correlations and impact on genetic counseling. *Hum Mutat*. 2007;28:81-91.
 52. Neidhardt J, Glaus E, Lorenz B, et al. Identification of novel mutations in X-linked retinitis pigmentosa families and implications for diagnostic testing. *Mol Vis*. 2008;14:1081-1093.